JCTC Journal of Chemical Theory and Computation

Article

pubs.acs.org/JCTC

Global ab Initio Potential Energy Surfaces for Low-Lying Doublet States of NO_3

Hongyan Xiao,[†] Satoshi Maeda,*[,‡] and Keiji Morokuma*[,†,§]

[†]Fukui Institute for Fundamental Chemistry, Kyoto University, 34-4 Takano Nishihiraki-cho, Sakyo, Kyoto 606-8103, Japan

[‡]Department of Chemistry, Faculty of Science, Hokkaido University, Sapporo, 060-0810, Japan

[§]Cherry L. Emerson Center for Scientific Computation and Department of Chemistry, Emory University, Atlanta, Georgia 30322, United States

Supporting Information

ABSTRACT: We report analytical global potential energy surfaces (PESs) for three low-lying doublet states (D_0, D_1, and D_2) of NO_3. The fits are made on roughly 74000 MS-CAS(17e,13o)PT2/aug-cc-pVTZ calculations of electronic energies, where these PESs are invariant of permutations of oxygen atoms. The surfaces describe two roaming pathways for $NO_3 \rightarrow NO_2$-----$O \rightarrow NO + O_2$ involving different electronic states discovered in the photolysis of NO_3 [Xiao, H. Y. et al. *J. Phys. Chem. Lett.* **2011**, *2*, 934]. These pathways become accessible at excess energy of ~210 kJ/mol above the ground-state global minimum of NO_3. The ab initio data below 360 kJ/mol are reproduced very well by the fitted PESs with the fitting rms errors of less than 5.5 kJ/mol for all the three states. Moreover, key local minima and energy profiles along the roaming pathways on the fitted PESs are compared with those on the ab initio PESs. In addition, potential contour maps in the roaming region are also compared. These careful evaluations of the fitted PESs suggest that the present fitted PESs are well suited for future dynamics calculations of this system.

1. INTRODUCTION

Since roaming was discovered in 2004 in the ground-state dynamics of the photolysis of formaldehyde (H_2CO),[1] the roaming mechanism has become a very popular topic in many chemical reaction dynamics, both theoretically and experimentally.[2−18] Roaming has been discussed exclusively for reactions on the ground electronic state and is often involved in minor channels of the reaction mechanism.

The original photodissociation experiment of the nitrate radical (NO_3) in a narrow wavelength range was reported by Magnotta and Johnston,[19] corresponding to 594.5−585.5 nm at 0 K.[20] Above the 585.5 nm threshold, the dissociated radical channel $NO_3 \rightarrow NO_2 + O$ was predominant, accounting for nearly 100% of the photoproducts. The 594.5 nm threshold for $NO_3 \rightarrow NO + O_2$ channel was assumed to arise from a concerted three-center transition state (TS).[21] North and co-workers[22,23] reported the presence of two distinct pathways for the formation of $NO + O_2$ at 588 nm by the velocity map ion imaging technique as follows.

$$NO_3 + \hbar\nu \rightarrow NO(^2\Pi_\Omega, \omega = 0{-}1, \text{low } J) + O_2\left(^3\Sigma_g^-, \omega = 5{-}10\right) \quad \text{major channel} \tag{a}$$

$$\rightarrow NO(^2\Pi_\Omega, \omega = 0{-}1, \text{high } J) + O_2(^3\Sigma_g^-, \omega = 0{-}4) \quad \text{minor channel} \tag{b}$$

where ω and J are the vibrational and rotational quantum numbers, respectively. A possibility of roaming dynamics has been suggested for the major channel, although the origin of the minor channel was not discussed.

Recently, on the basis of theoretical calculations consisting of a systematic MS-CAS(11e,8o)PT2/6-31+G* reaction path search and DFT dynamics calculations, we have proposed for photolysis of NO_3 the roaming pathway that takes place on an excited electronic state, as illustrated in Figure 1.[24] These

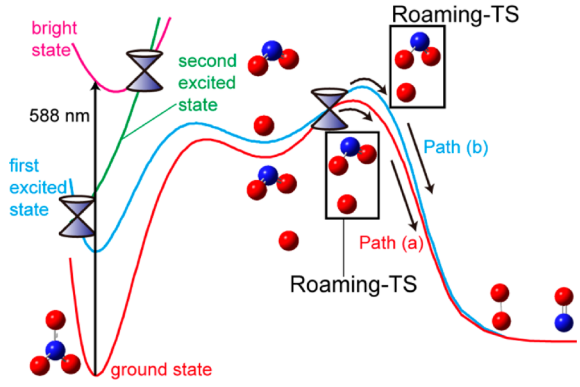

Figure 1. Potential energy surfaces and proposed reaction pathways for photodissociation of NO_3.

calculations showed that, after photoexcitation, the roaming dynamics takes place on the first excited doublet state (D_1), and then two pathways can take place: the direct dissociation on D_1 and the dissociation after nonadiabatic transition to the ground doublet state (D_0) via D_1/D_0 conical intersection. Direct DFT trajectory calculations from the dissociation TS on the D_1 state gave vibrationally cold O_2, while those from the dissociation TS on the D_0 state gave vibrationally hot O_2. This proposal of the two distinct channels explained North's experimental results and provided the first example of roaming dynamics that

Received: May 19, 2012
Published: July 3, 2012

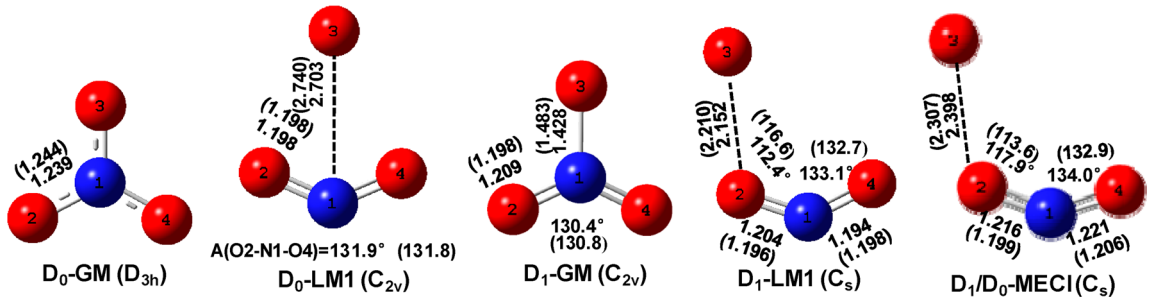

Figure 2. Optimized geometries of minima and minimum energy CI points on the ab initio MS-CASPT2 and the fit values (in the parentheses). Bond distance is in angstroms and angle in degrees.

occurred on an excited electronic state and exclusively without any other competing nonroaming channel.

Very recently a joint experimental and theoretical work[25] proved the exclusive excited-state roaming pathway that eventually produced two different product channels. The theoretical studies predicted specific NO Λ doublet propensities, namely, orientations of the unpaired electron with respect to the molecular rotation plane for the two product channels. The experimental studies using the ion imaging technique via multiple rotational branches proved that the major product channel with a high O_2 vibrational excitation produced a lower translational energy NO fragment in the A′ Λ doublet state, while the minor product channel with a low O_2 vibrational excitation produced a higher translational energy NO fragment in the A′′ Λ doublet state, confirming the theoretical predictions. North and coworkers further explored the stereodynamics of multistate roaming in the reaction of $NO_3 \rightarrow NO + O_2$.[26]

To fully support the theoretical conclusions derived from potential energy surface (PES) characteristics and limited classical dynamics from dissociation transition states, it is highly desirable to perform classical and hopefully quantum dynamics calculations for complete evolution of the system from photoexcitation in the Franck−Condon region through succeeding nonadiabatic and dissociation processes to the product. To make this possible, it is essential to have full PESs of multiple electronic states involved at a level higher than that used in our previous reaction path characterization study.[24] In particular, we are concerned with a small active space (11e,8o) used in such a study, which might have resulted in some errors in the very flat PESs in the roaming region as well as dissociation transition states.

In the present work, we develop such analytical global PESs for NO_3 on the basis of multistate (MS)-CAS(17e,13o)PT2/aug-cc-pVTZ ab initio calculations. The three lowest doublet state PESs (D_0, D_1 and D_2) are fitted, and the properties of the fitted PESs are evaluated.

2. AB INITIO CALCULATION AND FITTING PROCEDURE

The electronic structure calculations were carried out by the multistate (MS)-CAS(17e,13o)PT2/aug-cc-pVTZ method using Molcas 7.4 and 7.6 programs.[27] Critical points, i.e., global minimum (GM), local minimum (LM) and minimum energy conical intersection (MECI) structures were also optimized at the same level by the global reaction route mapping (GRRM) program[28] in which energies and gradient vectors were computed using Molcas 7.4 program as an external subroutine. An MECI on the ab initio PES was optimized by the direct gradient method[29] and the branching-plane updating method.[30] The choice of the active space was based on the previous theoretical work;[31−33] to keep the geometry for the NO_3 global minimum in the D_{3h} symmetry, at least the (17e,13o) active space is required. The three-state averaging was employed with equal weight for the first three doublet states (D_0, D_1, and D_2) in the reference CASSCF calculations. The shift parameter 0.3 was applied in the CASPT2 calculations to avoid the intruder state problem.[34]

On the basis of the MS-CASPT2 calculations, the D_0, D_1, and D_2 PESs were fitted. First, the structures (see Figure 2 in ref 24) of roughly 350 points were sampled along the intrinsic reaction coordinates (IRCs) obtained in the previous small active space calculations. Then, we calculated a series of structures of NO_2 by the MS-CAS(17e,12o)/aug-cc-pVTZ method. On the basis of lower energy structures of NO_2, we set up the initial loose grids, i.e., the roaming O atom with coordinate increments of 0.5 Å around a series of lower energy structures of NO_2 in the 10 × 10 × 10 Å^3 box, and then chose the lower energy structures among the loose grids to further set up fine grids (the roaming O coordinate increment of 0.2 Å) in the 8 × 8 × 8 Å^3 box, where the center of mass of NO_2 was regarded as the origin. About 63350 ab initio energies were used in the initial fit. On the fitted PESs, global reaction route mapping was performed by the GRRM method to find out strange local minima or deep (unphysical) "holes" generated by the error of the fits, because such strange minima may distort the dynamics. If such a minimum was located and was found to be accessible from the GM on each surface within an excess energy of 360 kJ/mol, ab initio energies were sampled along all IRCs leading to the strange minimum and then the PESs were refitted. This search-and-sample-and-refit procedure was repeated until no such a minimum was found. As described in our previous papers,[35−37] the GRRM method can locate all local minima and first-order saddle points on a given function. Thus, the final fitted PESs do not have any strange minimum in the region accessible with the 360 kJ/mol excess energy. As a result, 74435 ab initio energies were computed in total.

The fitting functional form of the potential is similar to the one used previously for fitting the H_2CO potential.[38] The PES is expanded with the Taylor series,

$$V = C_0 + \sum_{i=1}^{6} C_{1i}q_i + \sum_{i=1}^{6}\sum_{j=1}^{6} C_{2ij}q_iq_j + \sum_{i=1}^{6}\sum_{j=1}^{6}\sum_{k=1}^{6} C_{3ijk}q_iq_jq_k + \ldots + \sum_{i=1}^{6}\sum_{j=1}^{6}\sum_{k=1}^{6}\sum_{l=1}^{6}\sum_{m=1}^{6}\cdots\sum_{n=1}^{6} C_{Nijklm\ldots n}q_iq_jq_kq_lq_m\cdots q_n$$

dx.doi.org/10.1021/ct3004035 | J. Chem. Theory Comput. 2012, 8, 2600−2605

Table 1. RMS Fitting Error and the Maximum Absolute Error (in kJ/mol) of the MS-CASPT2 Fit as a Function of Energy Range (E_{max} = 360 kJ/mol)[a,b]

	D_0		D_1		D_2	
energy range	rms	sample points	rms	sample points	rms	sample points
0−360	5.5(39.9)	74435	5.4(35.3)	70873	3.8(33.9)	59029
0−300	4.4(39.9)	52812	4.3(35.3)	49056	2.7(30.8)	39262
0−250	3.6(34.8)	38599	3.3(29.9)	34996	2.1(28.8)	25718
0−200	4.8(34.8)	8170	4.8(29.4)	5690	3.5(24.2)	3057
0−150	3.9(27.9)	5639	4.0(29.4)	4215	2.6(14.5)	2523

[a]The value in parentheses is the maximum absolute error in the given energy range. [b]The number of ab initio (sample) points in the given energy range is also given.

Table 2. Absolute (E_A) and Relative (E_R) Energies of the Critical Points from ab Initio MS-CASPT2 and the Fit

	ab initio CASPT2		fit	
state	E_A (Hartree)	E_R (kJ/mol)	E_A (Hartree)	E_R (kJ/mol)
D_0-GM	−279.8313292	0.0	−279.8315994	0.0
D_0-LM	−279.7520028	208.3	−279.7519463	209.1
D_1-GM	−279.7980133	87.5	−279.7966552	91.7
D_1-LM	−279.7514658	209.7	−279.7519910	209.0
D_1/D_0-MECI	−279.7497377	214.2	−279.7517379	209.7

or equivalently

$$V = \sum_{a=0}\sum_{b=0}\sum_{c=0}\sum_{d=0}\sum_{e=0}\sum_{f=0} c_{abcdef} q_1^a q_2^b q_3^c q_4^d q_5^e q_6^f,$$

$$a + b + c + d + e + f \le N$$

$$q_i = 1 - \exp\left[-\alpha\left(\frac{r_i}{sr_0} - 1\right)\right]$$

where the Morse function q_i is the variable and N is the polynomial order. Taylor series coefficients ($C_{Nijklm..n}$ or c_{abcdef}) are determined by the standard linear least-squares fitting method. Because of the O atom permutations, some of Taylor series coefficients should have the same values and are restricted to be identical during the fit. In other words, the final PESs are fully invariant of permutations of O atoms. In the present work, the polynomial was truncated at the 7th order, where 343 coefficients are independent among a total of 1716 coefficients. In the Morse function, r_i is the i th internuclear distance between two atoms, where all the six atom−atom pairs among the four atoms in NO_3 were considered as r_i, r_0 is a corresponding equilibrium distance represented by the sum of covalent radii, s is a scaling factor of r_0 and set to 1.2, and α was set to 1.0 in the present work.

It should be noted that the three PESs were fitted independently. In other words, these three PESs do not cross exactly. One MECI shown below between the D_0 and D_1 surfaces was optimized by a penalty function type MECI-optimizer,[16] and hence there still is a subtle energy gap at this point. However, the gap is only 0.01 kJ/mol, and the two PESs nearly touch each other at this point.

3. RESULTS AND DISCUSSION

The final values of the 343 independent corresponding Taylor expansion coefficients are given in the Supporting Information. The code for analytical potential functions together with their gradients is available upon request.

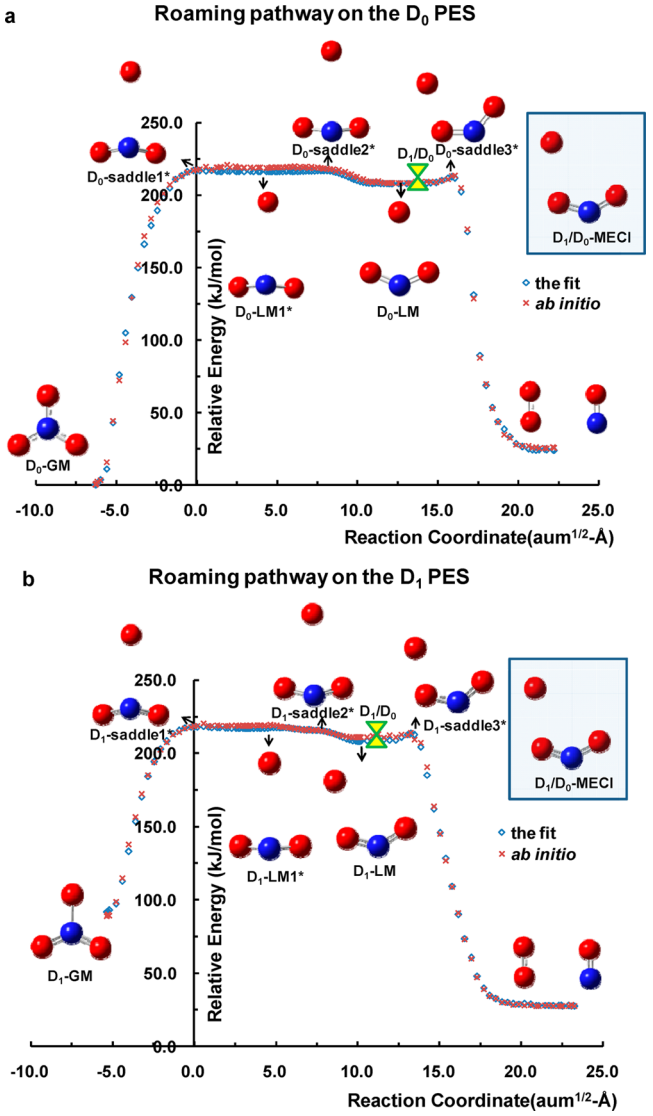

Figure 3. Roaming pathways on the D_0 and D_1 PESs (a and b) from ab initio MS-CASPT2 and the fit.

3.1. Fitting rms Errors. In the present work a total of 74435 ab initio energies below 360 kJ/mol (all the energies are relative to the one of the global minimum on the D_0 state) were used in the fit. The accuracy of the fit was determined by the root-mean-square (rms) error as well as the maximum absolute error as functions of maximum energy E_{max} used in the fit, as shown in Table 1.

As seen in Table 1, the fitting errors are very small; for the data below 360 kJ/mol, the rms errors are only ~5.5 kJ/mol for

dx.doi.org/10.1021/ct3004035 | J. Chem. Theory Comput. 2012, 8, 2600−2605

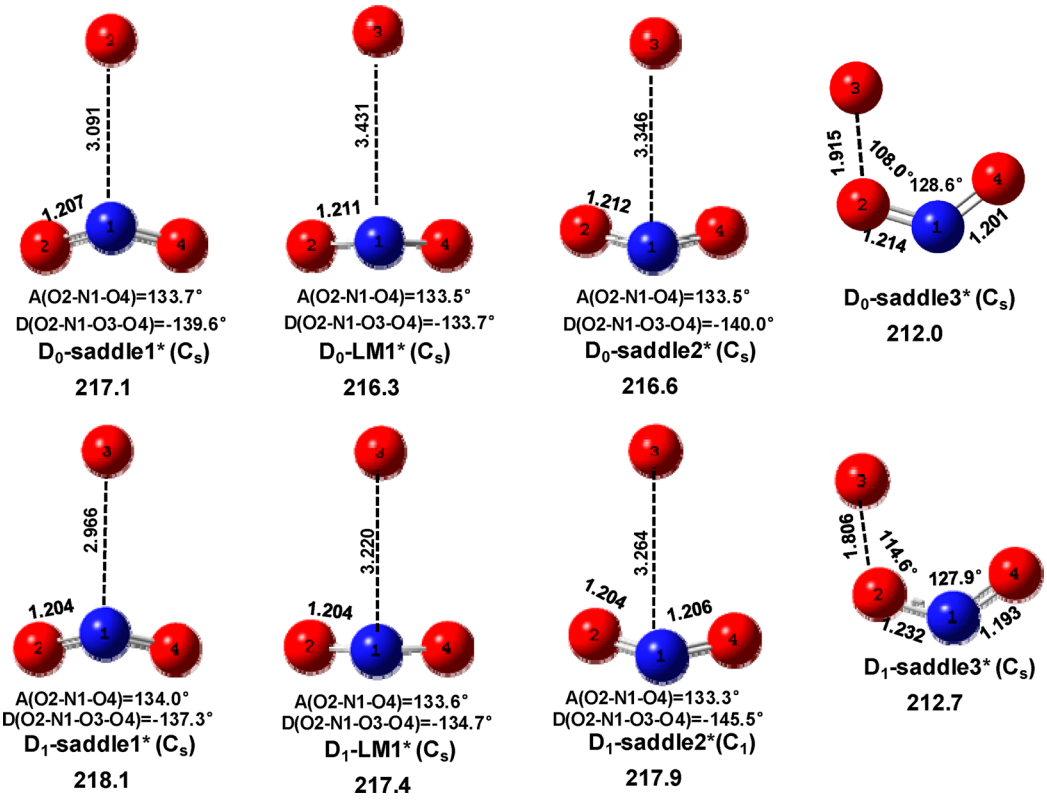

Figure 4. The structures and relative energies (in kJ/mol) of some key points on the fitted PESs. Bond distance is in angstroms, and angle in degrees.

all the three states. These rms values are similar to those reported for the ground-state PES of H_2CO.[38] Thus, the present PESs are accurate enough at least in the vicinity of the 74435 sampling points.

3.2. Structures and Energies at Minimum Energy Points. A comparison of the geometries and energies of the global minima, local minima, and an MECI for the ground and the first excited doublet states (D_0-GM, D_1-GM, D_0-LM, D_1-LM, D_1/D_0-MECI) from the fitted potential functions and directly from the ab initio MS-CASPT2 calculations is given in Figure 2 and Table 2.

As seen in Figure 2, geometrical parameters were reproduced very well with maximum errors of 0.058 Å and 4.2° for minima. The errors in the MECI are still acceptable, although these are a little larger than those for minima because of the treatment to fit the three PESs independently. In Table 2, the maximum error in the relative energy of 4.5 kJ/mol is seen in the D_1/D_0-MECI, which is also small. Hence, the fitted PESs are also reliable around these minimum energy points.

3.3. Two Roaming Pathways on the D_0 and D_1 PESs. Because of the very flat PESs in the roaming region, it is very difficult to find all reaction pathways in this region. Moreover, optimization of saddle points at the MS-CAS(17e,13o)PT2/aug-cc-pVTZ level is highly demanding because numerical Hessian calculations are required. Fortunately, we were able to employ the fitted PESs in the exhaustive search by the GRRM method and determine the two distinct pathways (pathways a and b), corresponding to roaming dynamics on the D_0 and D_1 states, respectively. As shown in Figure 3, several saddle points and local minima were found along the minimum energy dissociation paths on the basis of the fitted PESs. Figure 4 gives the structures and relative energies of the corresponding stationary points on the fitted PESs, except for those shown in Figure 2. To show how well the fitted PESs reproduce the energy profile along these paths, we evaluated ab initio electronic energies at the MS-CAS(17e,13o)PT2/aug-cc-pVTZ level using many points along these minimum energy paths on the fitted PESs.

As seen in Figure 3, along these IRCs the ab initio MS-CASPT2 energy curves correspond with the fitting curves on the D_0 and D_1 states well; the plots of these surfaces are nearly overlapping in the roaming (flat) region. In comparison with our previous results[24] using the small active space MS-CAS(11e,8o)PT2/6-31+G* method, the roaming regions of the PESs are much more flat in the present results. This is due to the small active space and the small basis set employed in the previous study, and the present results are much more reliable. Despite the change in the flatness of the roaming regions of the PESs, the most important trends remain. On the fitted PESs, the O−O distance between the recombining oxygen atoms at D_0-saddle3* is 1.915 Å which is longer than the one at D_1-saddle3*, 1.806 Å. This difference in the O−O distances is the cause of the different vibrational excitation in the O_2 products produced on the different surfaces. In conclusion, the accuracy of the fitted PESs is acceptable along the roaming pathways as well. In comparison with the experimental dissociation threshold (594.5−585.8 nm, i.e., 201.2−204.3 kJ/mol) for $NO_3 \rightarrow NO + O_2$, the dissociation threshold from both the fitted and ab initio PESs is larger by ∼10 kJ/mol because the zero point vibrational energy is not included in PESs.

3.4. Contour Plots of the D_0, D_1, and D_2 PESs. In general, many trajectories of roaming dynamics pass through regions largely deviated from the corresponding minimum energy path. The fitted PESs should be accurate in a wide area. Hence, we compared contour plots of the fitted and ab initio PESs in this section.

In the roaming region as shown in Figures 3 and 4, one finds a common structural characteristic, i.e., ∼133° of the O2−N1−O4 angle. Although the whole roaming region covers noncoplanar

dx.doi.org/10.1021/ct3004035 | J. Chem. Theory Comput. 2012, 8, 2600−2605

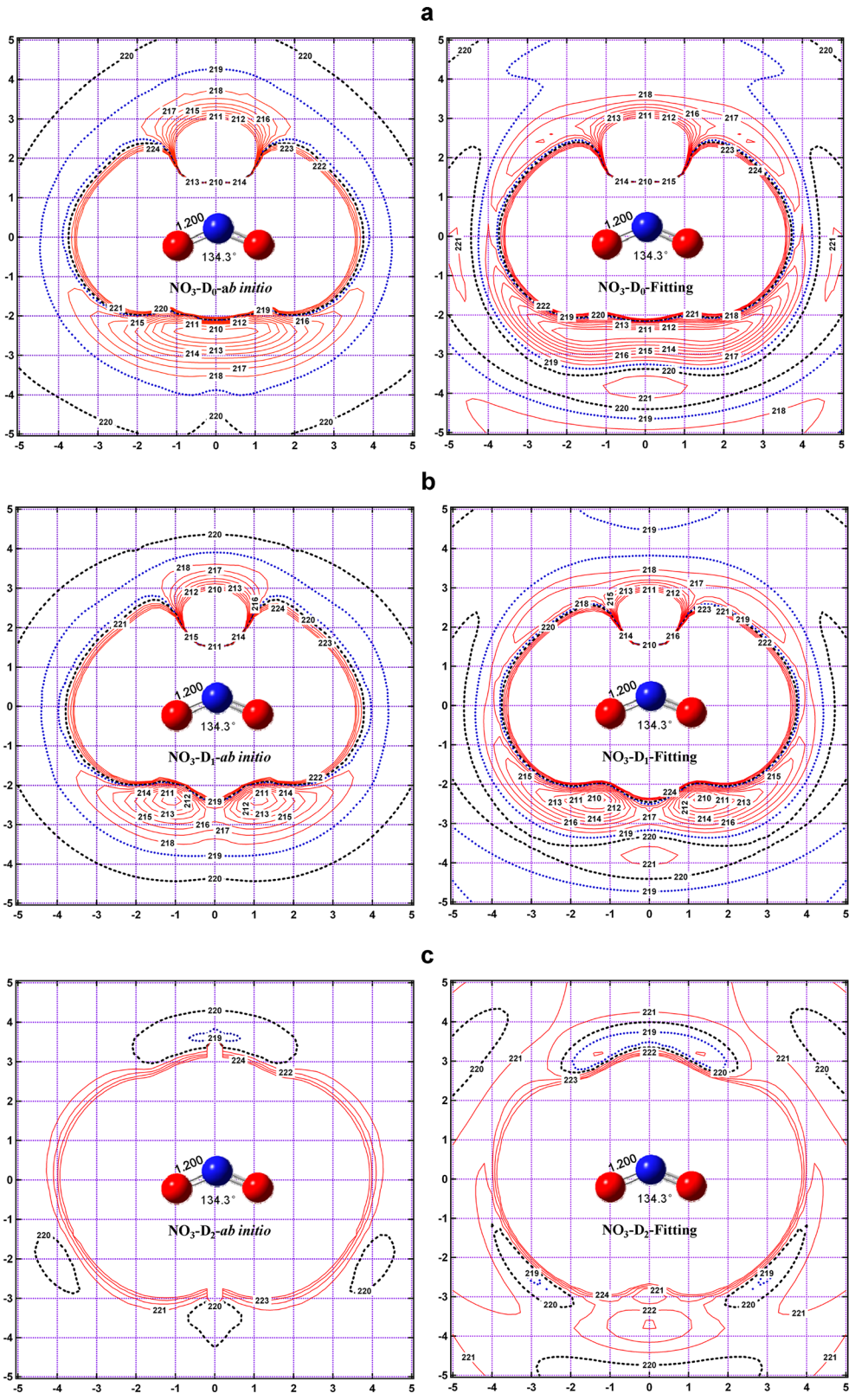

Figure 5. Contour plots as functions of coordinates (in angstroms) of another O atom on the D_0, D_1, and D_2 states (a, b, and c) from the ab initio MS-CASPT2 and the fit, where the NO_2 fragment is fixed at its global minimum.

structures, the final O_2 exit channels on the D_0 and D_1 PESs are on the O2−N1−O4 molecular plane; for instance, see the path D_0-LM (C_{2v}) → D_0-saddle3* (planar C_s) → NO + O_2 as well as the path D_1-LM (planar C_s) → D_1-saddle3* (planar C_s) → NO + O_2. Considering the above two points, we compared the planar contour plots for the three low-lying doublet states of NO_3 from the ab initio PESs and the fit in Figure 5. The O−N−O angle is set to 134.3° and O−N bond distance to 1.200 Å, of which NO_2 global minimum is at the MS-CAS(17e,12o)PT2/aug-cc-pVTZ level. The position of the roaming O atom is on the plane around

dx.doi.org/10.1021/ct3004035 | J. Chem. Theory Comput. 2012, 8, 2600−2605

the NO_2 fragment. In Figure 5, shallow minimum energy paths are seen in the energy range of 219−220 kJ/mol on the D_0 and D_1 PESs; along them the partially dissociated O atom can migrate. On the other hand, the O atom potential is repulsive on the D_2 state.

We also considered contour plots with various different NO_2 geometries. One with the NO_2 fragment fixed in the Franck−Condon point of NO_3 and another with the NO_2 fragment at a structure similar to the two saddles of the O_2 exit channels on the D_0 and D_1 PESs are shown in Figures S1 and S2 of Supporting Information. As a whole, the contour plots on the D_0, D_1, and D_2 PESs of NO_3 from the fit are in good agreement with those from ab initio MS-CASPT2 with the energy values below 360 kJ/mol.

4. SUMMARY

Analytical global potential energy surfaces for the three low-lying doublet states of NO_3 have been constructed by fitting roughly 74000 MS-CAS(17e,13o)PT2/aug-cc-pVTZ calculations of electronic energies. In comparison with the ab initio results, the rms errors of three states, five key minima, two roaming pathways on the D_0 and D_1 states, and contour plots of the three PESs were described well based on the fitted PESs for energies up to 360 kJ/mol. The present fitted PESs are well suited for future dynamics calculations of this system.

■ ASSOCIATED CONTENT

Ⓢ Supporting Information

Taylor expansion coefficients and contour plots from the different NO_2 fragments. This material is available free of charge via the Internet at http://pubs.acs.org.

■ AUTHOR INFORMATION

Corresponding Author

*E-mail: smaeda@mail.sci.hokudai.ac.jp (S.M.); keiji.morokuma@emory.edu (K.M.).

Notes

The authors declare no competing financial interest.

■ ACKNOWLEDGMENTS

This work is partly supported by a grant from Japan Science and Technology Agency with a Core Research for Evolutional Science and Technology (CREST) in the Area of High Performance Computing for Multiscale and Multiphysics Phenomena at Kyoto University, a grant from Japan Society for the Promotion of Science (Grants-in-Aid for Scientific Research <KAKENHI> No. 23685004) at Hokkaido University, and a grant from US AFOSR (Grant No. FA9550-10-1-0304) at Emory University. A majority of single-point CASPT2 calculations were performed using the computational resources at Institute for Molecular Science, Okazaki, Japan.

■ REFERENCES

(1) Townsend, D.; Lahankar, S. A.; Lee, S. K.; Chambreau, S. D.; Suits, A. G.; Zhang, X.; Rheinecker, J.; Harding, L. B.; Bowman, J. M. *Science* **2004**, *306*, 1158−1161.

(2) Bowman, J. M.; Zhang, X. *Phys. Chem. Chem. Phys.* **2006**, *8*, 321−332.

(3) Suits, A. G. *Acc. Chem. Res.* **2008**, *41*, 873−881.

(4) Herath, N.; Suits, A. G. *J. Phys. Chem. Lett.* **2011**, *2*, 642−647.

(5) Bowman, J. M.; Shepler, B. C. *Annu. Rev. Phys. Chem.* **2011**, *62*, 531−553.

(6) Houston, P. L.; Kable, S. H. *Proc. Natl. Acad. Sci. U.S.A.* **2006**, *103*, 16079−16082.

(7) Shepler, B. C.; Braams, B. J.; Bowman, J. M. *J. Phys. Chem. A* **2007**, *111*, 8282−8285.

(8) Heazlewood, B. R.; Jordan, M. J. T.; Kable, S. H.; Selby, T. M.; Osborn, D. L.; Shepler, B. C.; Braams, B. J.; Bowman, J. M. *Proc. Natl. Acad. Sci. U.S.A.* **2008**, *105*, 12719−12724.

(9) Goncharov, V.; Herath, N.; Suits, A. G. *J. Phys. Chem. A* **2008**, *112*, 9423−9428.

(10) Chen, C.; Braams, B.; Lee, D. Y.; Bowman, J. M.; Houston, P. L.; Stranges, D. *J. Phys. Chem. Lett.* **2010**, *1*, 1875−1880.

(11) Kamarchik, E.; Koziol, L.; Reisler, H.; Bowman, J. M.; Krylov, A. I. *J. Phys. Chem. Lett.* **2010**, *1*, 3058−3065.

(12) Fernández-Ramos, A.; Miller, J. A.; Klippenstein, S. J.; Truhlar, D. G. *Chem. Rev.* **2006**, *106*, 4518−4584.

(13) Harding, L. B.; Klippenstein, S. J.; Jasper, A. W. *Phys. Chem. Chem. Phys.* **2007**, *9*, 4055−4070.

(14) Harding, L. B.; Klippenstein, S. J. *J. Phys. Chem. Lett.* **2010**, *1*, 3016−3020.

(15) Zhang, P.; Maeda, S.; Braams, B. J.; Morokuma, K. *J. Chem. Phys.* **2009**, *130*, 114304.

(16) Maeda, S.; Ohno, K.; Morokuma, K. *J. Phys. Chem. A* **2009**, *113*, 1704−1710.

(17) Maeda, S.; Ohno, K.; Morokuma, K. *Adv. Phys. Chem.* **2012**, *2012*, 268124.

(18) Hause, M. L.; Herath, N.; Zhu, R.; Lin, M. C.; Suits, A. G. *Nat. Chem.* **2011**, *3*, 932−937.

(19) Magnotta, F.; Johnston, H. S. *Geophys. Res. Lett.* **1980**, *7*, 769−772.

(20) Johnston, H. S.; Davis, H. F.; Lee, Y. T. *J. Phys. Chem.* **1996**, *100*, 4713−4723.

(21) Mikhaylichenko, K.; Riehn, C.; Valachovic, L.; Sanov, A.; Wittig, C. *J. Chem. Phys.* **1996**, *105*, 6807−6817.

(22) Grubb, M. P.; Warter, M. L.; Suits, A. G.; North, S. W. *J. Phys. Chem. Lett.* **2010**, *1*, 2455−2458.

(23) Grubb, M. P.; Warter, M. L.; Johnson, K. M.; North, S. W. *J. Phys. Chem. A* **2011**, *115*, 3218−3226.

(24) Xiao, H. Y.; Maeda, S.; Morokuma, K. *J. Phys. Chem. Lett.* **2011**, *2*, 934−938.

(25) Grubb, M. P.; Warter, M. L.; Xiao, H. Y.; Maeda, S.; Morokuma, K.; North, S. W. *Science* **2012**, *335*, 1075−1078.

(26) Grubb, M. P.; Warter, M. L.; North, S. W. *Phys. Chem. Chem. Phys.* **2012**, *14*, 6733−6740.

(27) Aquilante, F.; Vico, L.; De; Ferre, N.; Ghigo, G.; Malmqvist, P.-Å; Neogrady, P.; Pedersen, T. B.; Pitonak, M.; Reiher, M.; Roos, B. O.; Serrano-Andres, L.; Urban, M.; Veryazov, V.; Lindh, R. *J. Comput. Chem.* **2010**, *31*, 224−247.

(28) Maeda, S.; Osada, Y.; Morokuma, K.; Ohno, K. GRRM, a developmental version, 2012 (see http://grrm.chem.tohoku.ac.jp/SRPS/GRRMe.HTM for the latest distributed version GRRM11, 2011).

(29) Bearpark, M. J.; Robb, M. A.; Schlegel, H. B. *Chem. Phys. Lett.* **1994**, *223*, 269−274.

(30) Maeda, S.; Ohno, K.; Morokuma, K. *J. Chem. Theory Comput.* **2010**, *6*, 1538−1545.

(31) Eisfeld, W.; Morokuma, K. *J. Chem. Phys.* **2000**, *113*, 5587−5597.

(32) Eisfeld, W.; Morokuma, K. *J. Chem. Phys.* **2001**, *114*, 9430−9440.

(33) Eisfeld, W.; Morokuma, K. *J. Chem. Phys.* **2003**, *119*, 4682−4688.

(34) Roos, B. O.; Andersson, K. *Chem. Phys. Lett.* **1995**, *245*, 215−223.

(35) Ohno, K.; Maeda, S. *Chem. Phys. Lett.* **2004**, *384*, 277−282.

(36) Maeda, S.; Ohno, K. *J. Phys. Chem. A* **2005**, *109*, 5742−5753.

(37) Ohno, K.; Maeda, S. *J. Phys. Chem. A* **2006**, *110*, 8933−8941.

(38) Zhang, X.; Zhou, S.; Harding, L. B.; Bowman, J. M. *J. Phys. Chem. A* **2004**, *108*, 8980−8986.